Unique Cellular Interaction of Silver Nanoparticles: Size-Dependent Generation of Reactive Oxygen Species

C. Carlson,[†] S. M. Hussain,*[,†] A. M. Schrand,[†] L. K. Braydich-Stolle,[†] K. L. Hess,[‡] R. L. Jones,[†] and J. J. Schlager[†]

Applied Biotechnology Branch, Human Effectiveness Directorate, and Science Applications International Corporation, Air Force Research Laboratory, Wright-Patterson Air Force Base, Dayton, Ohio 45433

Received: December 26, 2007; Revised Manuscript Received: June 19, 2008

The rapid advancement of nanotechnology has created a vast array of engineered nanomaterials (ENMs) which have unique physical (size, shape, crystallinity, surface charge) and chemical (surface coating, elemental composition and solubility) attributes. These physicochemical properties of ENMs can produce chemical conditions to induce a pro-oxidant environment in the cells, causing an imbalanced cellular energy system dependent on redox potential and thereby leading to adverse biological consequences, ranging from the initiation of inflammatory pathways through to cell death. The present study was designed to evaluate size-dependent cellular interactions of known biologically active silver nanoparticles (NPs, Ag-15nm, Ag-30nm, and Ag-55nm). Alveolar macrophages provide the first defense and were studied for their potential role in initiating oxidative stress. Cell exposure produced morphologically abnormal sizes and adherence characteristics with significant NP uptake at high doses after 24 h. Toxicity evaluations using mitochondrial and cell membrane viability along with reactive oxygen species (ROS) were performed. After 24 h of exposure, viability metrics significantly decreased with increasing dose (10−75 μg/mL) of Ag-15nm and Ag-30nm NPs. A more than 10-fold increase of ROS levels in cells exposed to 50 μg/mL Ag-15nm suggests that the cytotoxicity of Ag-15nm is likely to be mediated through oxidative stress. In addition, activation of the release of traditional inflammatory mediators were examined by measuring levels of cytokines/chemokines, including tumor necrosis factor (TNF-α), macrophage inhibitory protein (MIP-2), and interleukin-6 (IL-6), released into the culture media. After 24 h of exposure to Ag-15nm nanoparticles, a significant inflammatory response was observed by the release of TNF-α, MIP-2, and IL-1β. However, there was no detectable level of IL-6 upon exposure to silver nanoparticles. In summary, a size-dependent toxicity was produced by silver nanoparticles, and one predominant mechanism of toxicity was found to be largely mediated through oxidative stress.

1. Introduction

Various types of nanomaterials exhibit novel electrical, catalytic, magnetic, mechanical, photonic, and thermal properties to aid in the creation of unique applications for commercial and military sectors. As we identify new uses for materials with these special properties, the number of products containing such nanomaterials and their possible applications continue to grow exponentially. Nanomaterials are already being used or tested in a wide range of consumer products such as sunscreens, composites, and medical and electronic devices, and they are also being used as chemical catalysts. Similarly to nanotechnology's success in consumer products and other sectors, nanomaterials also have promising environmental impact applications.[1−3] For example, nanosized cerium oxide has been developed to decrease diesel emissions, and iron nanoparticles can remove contaminants from soil and groundwater. Nanosized sensors hold promise for improved detection and tracking of contaminants. However, some of the same special properties that make nanomaterials useful are also properties that can cause some hazards to humans and the environment.[4,5] Of course, because of their small size, nanoparticles can enter plant or animal tissues and can easily pass through cell membranes such as the blood−brain barrier to critical areas within the brain or to other organs or tissue.[6] Inhaled nanoparticles easily suspended in air can be respired and become lodged in the lung, causing significant amounts of cell damage. High-durability nanomaterials raise issues of their residence time and overall fate in the environment.

Silver nanometal has been used in many consumer applications, mostly because of its well-demonstrated and safe use as an antimicrobial agent.[7−9] Silver nanoparticles in the sub-50-nm range exhibit increased efficacy in inhibiting a wide range of bacteria and fungi. Although silver nanoparticles are already found widely in multiple products, a concrete assessment of silver nanoparticles regarding effects on human health and environmental implications remains lacking. Because of the strong affinity of silver with redox-reactive and protective −SH groups,[10] it is possible that nanosilver could pose a threat to the balance of human health. The toxicity of silver exhibited in liver cells was also shown to be mediated by oxidative stress,[11] and silver nanoparticles were found to induce toxicity in germline stem cells.[12] Further information on the basic toxicity of nanosized metals such as silver is needed in terms of their interactions with cellular receptors, extra-/intracellular proteins, organelles, and DNA. A major acute exposure toxicological

* Address for correspondence: Saber Hussain, Ph.D., Research Toxicologist, Applied Biotechnology Branch, Air Force Research Laboratory/711th Human Systems Wing, AFRL/RHPB, Area B, R ST, BLDG 837, Wright Patterson Air Force Base, AFB, Dayton, OH 45433-5707. Tel.: 937-904-9517. Fax: 937-904-9610. E-mail: saber.hussain@wpafb.af.mil.

[†] Applied Biotechnology Branch, Human Effectiveness Directorate.

[‡] Science Applications International Corporation, Air Force Research Laboratory.

10.1021/jp712087m CCC: $40.75
Published on Web 10/03/2008

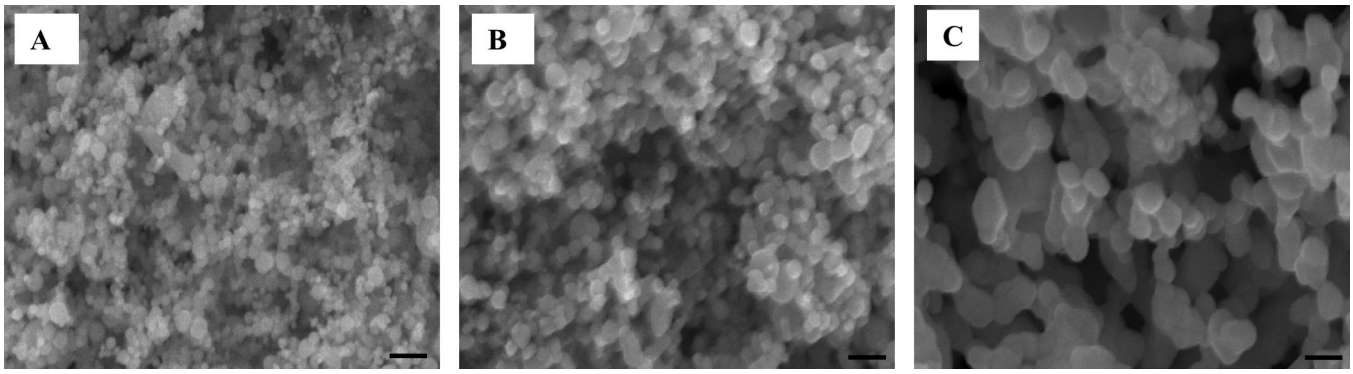

Figure 1. Characterization of Ag nanoparticle size and morphology with scanning electron microscopy (SEM). Images of Ag nanoparticles from Nanotechnologies, Inc., showing the spherical morphologies that increase in average size between samples. (A) Ag-15nm, (B) Ag-30nm, and (C) Ag-55nm. Scale bars are 100 nm.

concern is derived from the redox-reactive nature of some manufactured nanomaterials[13] and their assumed ability to easily cross cell membranes into critical organelles such as mitochondria.[6] A recent study by Oberdorster et al. indicated that fullerene (C_{60}) induces oxidative stress in a fish model.[14] Although limited studies have been conducted on the toxicity of nanoparticles, there are increasing numbers of reports using in vitro models to evaluate potential toxicity screening of nanomaterials and their mechanism of action.

Exposure to nanoparticles is likely to occur through inhalation, dermal contact, and ingestion. Deposition of inhaled particulate matter has been found to be dependent on size. Consequently, silver nanoparticles are likely to have an effect on the deep regions of the lung, particularly the alveolar region.[15] Therefore, in the present study, rat alveolar macrophages were selected as a model cell line to assess the degree of toxicity and explore possible physical-/chemical-induced biomechanisms of toxicity after inhalation. Macrophages are generally a population of ubiquitously distributed mononuclear phagocytes responsible for numerous homeostatic, immunological, and inflammatory processes. A primary function is to act as foreign scavengers, roaming the lungs and engulfing foreign and potentially dangerous matter. Alveolar macrophages are known to be extremely effective in clearing foreign matter by internalizing particulates via phagocytosis and endocytosis.[16,17] The current study was designed to model nanoparticle exposure through inhalation by utilizing a cultured model of rat alveolar macrophages and to provide a general evaluation of silver nanoparticle toxicity.[4,5] In addition, several cellular mechanisms stemming from nanoparticle-induced toxicity, including oxidative stress and inflammatory and immunological responses, are evaluated.

2. Materials and Methods

2.1. Chemicals. Hydrocarbon-coated silver (15, 30, and 55 nm) were generously provided by Dr. Karl Martin, NovaCentrix Co. (formerly Nanotechnologies, Inc., Austin, TX). Synthesis of Ag nanoparticles used the same process to deactivate the surface. Surface coatings were independently examined by atomic absorption spectroscopy (AAS) and combustion techniques for any trace impurities (none were found). The thickness of the hydrocarbon coating was estimated to be ~2 nm by transmission electron microscopy (TEM), and an amorphous structure was verified by X-ray diffraction by the manufacturer. The surface hydrocarbon coating was applied as part of the manufacturing process to prevent nanoparticle (NP) sintering during plasma synthesis, not specifically for biological deactivation, and to maintain a constant coating in aqueous solutions. Titanium dioxide (TiO_2) nanoparticles were generously provided by Dr. Pratim Biswas' group in the Department of Chemical Engineering, Washington University, St. Louis, MO. Rat alveolar macrophages (NR8383 CRL-2192), Ham's Nutrient Mixture F-12K (Kaughn's Modification), and normal fetal bovine serum (FBS) were purchased from ATCC (Manassas, VA). Penicillin/streptomycin and 3-(4,5-dimethylthiazol-2-yl)-2,5-diphenyltetrazolium bromide (MTT) were purchased from Sigma Chemical Company (St. Louis, MO). Phosphate-buffered saline (10×, pH 7.4) and 2.5% trypsin were purchased from Gibco Invitrogen Corporation (Carlsbad, CA). Rat tail collagen (type 1) was purchased from UPSTATE (Waltham, MA). Dichlorofluorescein diacetate (DCFH-DA) was purchased from Molecular Probes (Carlsbad, CA). ELISA kits measuring cytokine levels were purchased from Biosource International (Camarilla, CA.).

2.2. Scanning Electron Microscopy (SEM) of Ag Nanoparticles. Scanning electron microscopy (SEM) characterization was performed on a Hitachi S-4800 field-emission instrument at an accelerating voltage of 15 kV. Dry Ag nanoparticles were dispersed on double-sided carbon adhesive tape onto an aluminum SEM stub and lightly dusted to release loose particles (Figure 1).

2.3. Dispersion of Nanomaterials in Solution. Dispersion tests were conducted in physiological phosphate-buffered saline (PBS), deionized water, dimethylsulfoxide (DMSO), and ethanol (EtOH) at a concentration of 10 mg/mL. Changes in pH, turbidity, and dispersion were observed following initial suspension and vigorous mixing with a touch vortexer or brief sonication for 5−10 s at 60 W. All of the Ag nanoparticles were insoluble in solution, and 10 mg/mL stock suspensions were then prepared based on the success of the dispersion and mixing tests. From these stock suspensions, various concentrations for exposure were prepared prior to each experiment in modified Ham's Nutrient Mixture F-12K supplemented with 10% FBS.

2.4. Cell Culture. Macrophages were grown in Ham's Nutrient Mixture F-12K (Kaughn's modification), pH 7.3, with 20% FBS (normal) and 1% antibiotic penicillin/streptomycin mixture. Cells were seeded or grown on rat tail type 1 collagen-coated flasks; 6-, 12-, or 96-well plates; or chamber slides and maintained in a 5% CO_2 incubator at 37 °C.

2.5. Treatment Protocol. For all experiments, cells were seeded to provide experimental stage 80% confluency in 6-, 12-, or 96-well plates or chamber slides and grown for 48−72 h. Upon reaching 80% adherent confluency, cells were treated with a range of concentrations of nanoparticles suspended in F-12K

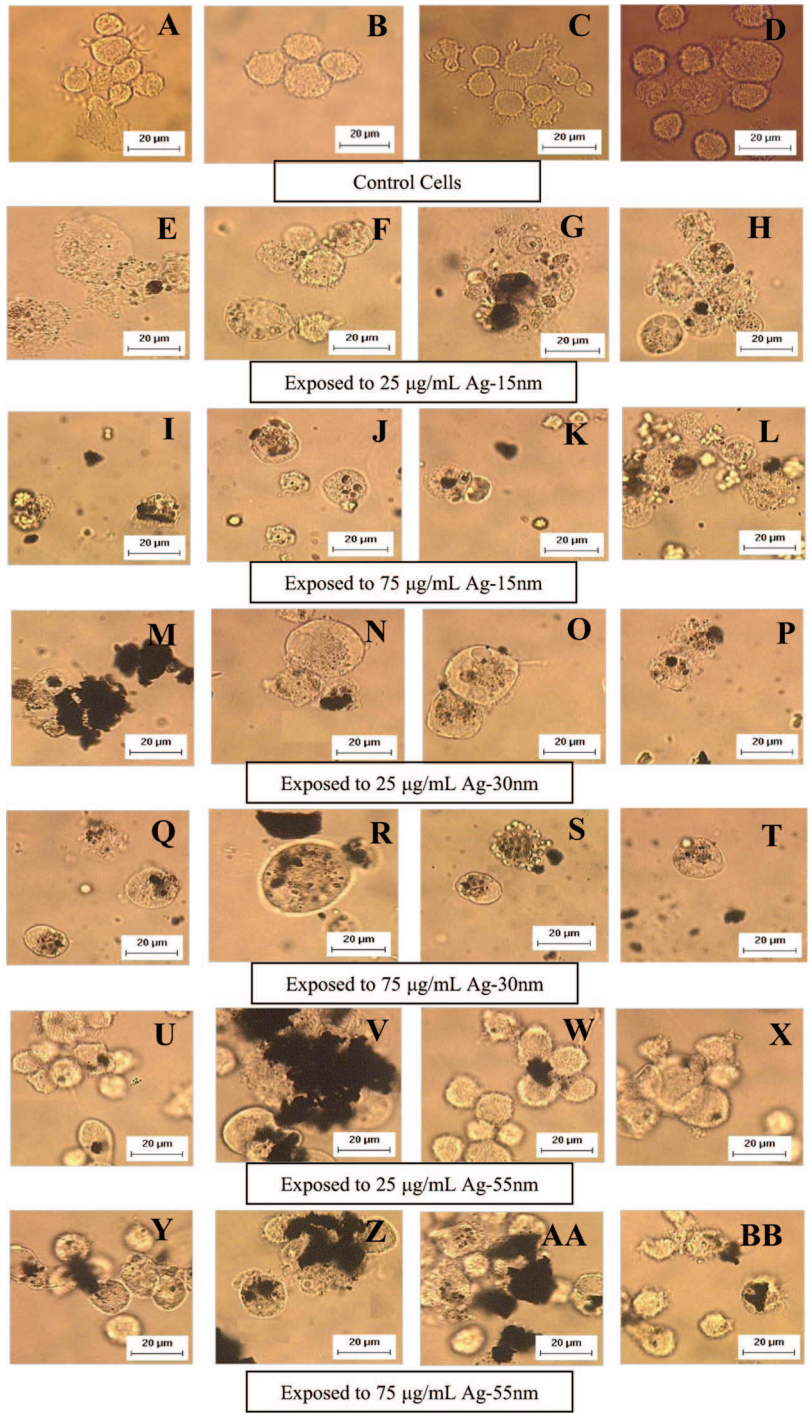

Figure 2. Inverted light microscopy (100×) of macrophages incubated with various concentrations of Ag nanoparticles for 24 h. (A−D) Control cells, (E−H) 25 μg/mL Ag-15nm, (I−L) 75 μg/mL Ag-15nm, (M−P) 25 μg/mL Ag-30nm, (Q−T) 75 μg/mL Ag-30nm, (U−X) 25 μg/mL Ag-55nm, and (Y−BB) 75 μg/mL Ag-55nm. Notice that most Ag nanoparticles show some form of agglomeration, with Ag-55nm displaying the most pronounced aggregates at both 25 and 75 μg/mL concentrations in images V and AA.

media with 10% serum for 24 h. At the end of the exposure period, toxicity end points were evaluated in control and nanoparticle-exposed cells.

2.6. Qualitative Observation of External Morphology by Phase-Contrast Inverted Microscopy. Rat alveolar macrophages were treated as mentioned above at various concentrations of nanoparticles for 24 h. After completion of the exposure period, the nanoparticle suspensions were removed, PBS was used to wash unbound nanoparticles from the cells, and then the cells were observed by inverted microscope (Olympus CK2) at 20× and 100× (oil) magnification (Figure 2). Images were captured via QCapture Pro Imaging Software.

2.7. Uptake of Ag NPs. Alveolar macrophages were grown to 80% confluency on dual-chamber slides under physiological conditions for 24−48 h and exposed under the same conditions as described in Treatment Protocol. After 24 h of exposure, excess medium was removed, and the cells were washed twice with PBS. Coverslips were placed over the slides and adhered with nail polish to prevent drying. Slides were inverted and observed with an Olympus IX71 microscope platform coupled with a CytoViva 150 Ultra Resolution Imaging (URI) system (Figure 3). Images were captured by QCapture Pro Imaging Software and stored with Microsoft PowerPoint and Microsoft Picture Manager. Nanoparticle-treated cells were also prepared

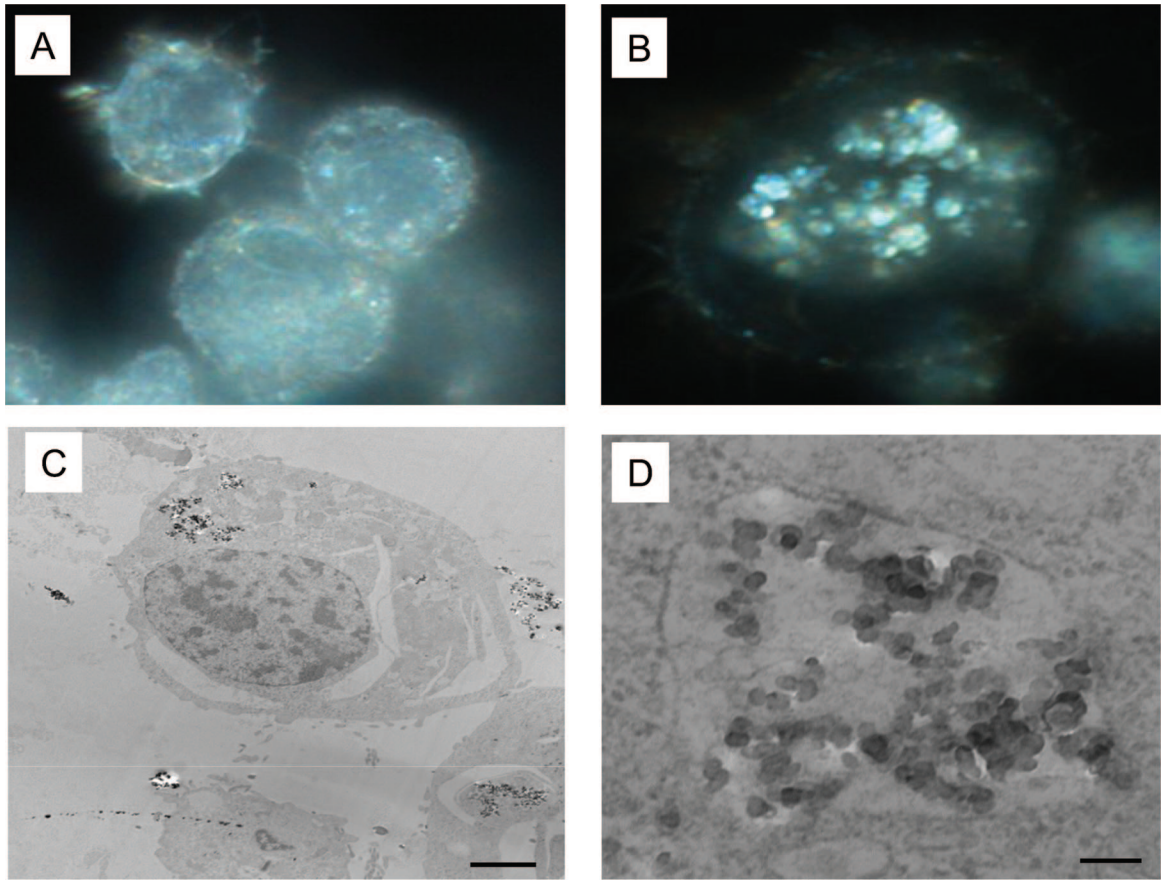

Figure 3. Examination of Ag nanoparticle uptake in macrophages. (A,B) CytoViva URI system light microscope images illustrating uptake of nanoparticles in alveolar macrophages at 100× oil magnification after 6 h. (A) Control (B) Cells treated with 25 μg/mL Ag-30nm. (C,D) Transmission electron microscopy (TEM) images showing (C) low-magnification overview of several cells that have internalized Ag nanoparticles into vacuoles after 24 h of incubation with 25 μg/mL Ag-55nm. Note that nanoparticles tend to be agglomerated in micron-sized clusters both inside and outside of the cells. (D) Higher-magnification image of lower cluster of Ag-55nm nanoparticles inside the large cell in C. Scale bars are (C) 2 μm and (D) 500 nm.

for TEM by fixation with paraformaldehyde, dehydration through a graded series of analytical grade ethanol, embedding in resin, thin sectioning, and staining with uranyl acetate/lead citrate. Images were recorded on a JEOL high-resolution transmission electron microscope at 80 kV (Figure 3).

2.8. Mitochondrial Function. Mitochondrial function was evaluated spectrophotometrically by measuring the degree of mitochondrial reduction of the tetrazolium salt 3-(4,5-dimethylthiazol-2-yl)-2,5-diphenyltetrazolium bromide (MTT) to formazan by succinic dehydrogenase.[18] Following exposure, cells were incubated with MTT salt for 20−30 min. The formation of a blue color marked the end of the incubation time, and the color was extracted with acidified isopropyl alcohol (IPA). The optical density (OD) of the extract was assayed with a SpectraMAX Plus 190 microplate reader at 570-nm wavelength and subtracted from 530-nm wavelength (Molecular Devices, Sunnyvale, CA) (Figure 4).

2.9. Membrane Integrity/LDH Leakage. Membrane integrity was assessed by measuring extracellular lactate dehydrogenase (LDH) according to the procedures described in the CytoTox-ONE Homogenous Membrane Integrity Assay kit. The kit provides a homogeneous, fluorometric method for measuring nonviable cells present based on the release of LDH. Fluorescence was measured at excitation and emission wavelengths of 560 and 590 nm, respectively, with a SpectraMAX Gemini Plus fluorescent microplate reader (Molecular Devices, Sunnyvale, CA). Data are reported as percentages of the control (Figure 5).

2.10. Reactive Oxygen Species (ROS) Generation. The reactive oxygen species (ROS) generation was determined using dichlorooffluorescein diacetate (DCFH-DA)[19] as previously described by Hussain et al. but with minor modifications.[31] Fluorescence values were measured in a 96-well plate using a SpectraMAX Gemini Plus fluorescent microplate reader (Molecular Devices, Sunnyvale, CA). Data are reported in terms of fold increase compared to a control (Figure 6).

2.11. GSH. Reduced glutathione (GSH) content was measured in 96-well plates using a SpectraMAX Plus 190 microplate reader (Molecular Devices, Sunnyvale, CA) according to the procedures describe in the Glutathione Assay Kit 703002 (Cayman Chemical Company, Ann Arbor, MI) (Table 2).

2.12. Mitochondrial Membrane Potential (MMP). Mitochondrial membrane permeability was determined using the Mit-E-Ψ Mitochondrial Permeability Detection Kit (BIOMOL, Plymouth Meeting, PA). Mit-E-Ψ reagent is the fluorescent cationic dye 5,5′,6,6′-tetrachlor-1,1′,3,3′- tetraethyl-benzamidazolocarbocyanin iodide, also known as JC-1. This dye reagent enters the mitochondria, aggregates, and fluoresces red. When the mitochondrial membrane potential collapses, the dye reagent can no longer accumulate within the mitochondria and fluoresces green. The rat alveolar macrophages were plated on chambered slides and a 96-well plate and treated with 0, 5, 25, and 50 μg/mL Ag-15nm, Ag-30nm, and Ag-55nm nanoparticles for 24 h. Following treatment, MMP was processed as per the manufacturer's instructions for imaging and fluorescent plate reader analysis, except that, for the plate reader analysis, instead

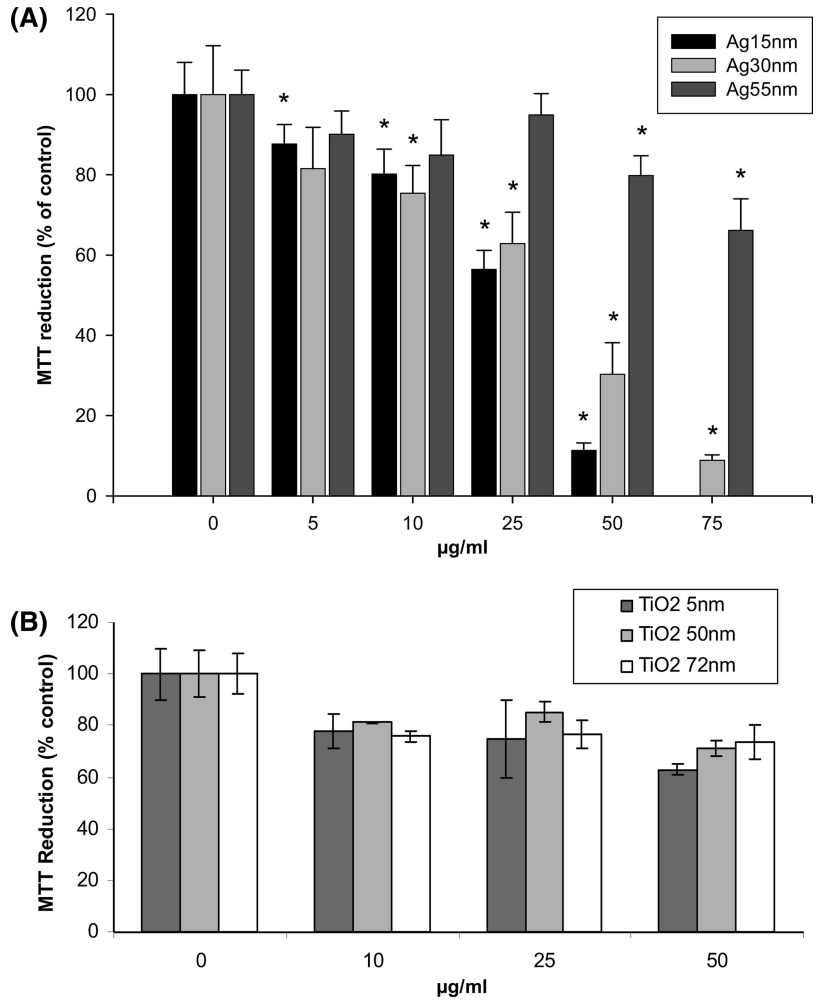

Figure 4. Effect of Ag and TiO_2 nanoparticles on mitochondrial function in macrophages. Mitochondrial function was assessed by the MTT reduction assay after 24 h of nanoparticle treatment. Optical density (OD) values were calculated as percentages of the OD measured in control cells (nanoparticle-free exposure media). The data are expressed as the mean ± standard deviation (SD) of three independent experiments conducted in triplicate. Asterisks (*) indicate a statistically significant difference compared to controls ($p < 0.05$). (A) Mitochondrial function was significantly reduced by Ag-15nm at concentrations starting from 5 μg/mL, by Ag-30nm starting from 10 μg/mL, and by Ag-55nm starting from 50 μg/mL, indicating a possible size-dependent cytotoxicity. (B) Negative nanoparticle control TiO_2 did not show any statistically significant difference compared to controls for any of the sizes examined.

of measuring the red/green ratio, only the green fluorescence measurement was used to determine the loss of mitochondrial membrane potential. The experiments were performed in triplicate, and data are expressed as averages ± the standard deviation (Figure 7). For the imaging studies, after 24 h of incubation, the macrophages were incubated with the Mit-E-Ψ reagent and the Hoescht 33342 vital nuclear stain. The macrophages were then imaged using a BD Pathway 435 confocal microscope with a 60× oil immersion lens. The nuclei of the cells were stained blue with the Hoescht 33342 stain, and the Mit-E-Ψ dye stained the healthy cells red and the apoptotic cells green. The macrophages were imaged with FITC, TRITC, and DAPI filters, and the images were merged to show the amount of green and red fluorescence in the cells. (Figure 8).

2.13. Inflammatory Response. Rat alveolar macrophages were exposed to 0, 5, 10, and 25 μg/mL Ag-15nm, Ag-30nm, or Ag-55nm nanoparticles for 24 h. Supernatants were collected 24 h after exposure and analyzed for secreted levels of TNF-α, MIP-2, IL-1β, and IL-6 by enzyme-linked immunosorbent assay (ELISA) analysis. ELISAs were conducted based on the manufacturer's instructions (BioSource International, Camarillo, CA) (Figure 9).

2.14. Statistical Evaluation. Wherever appropriate, the data were subjected to statistical analysis by one-way analysis of variance (ANOVA) followed by Tukey−Kramer's procedure for multiple comparisons. A value of $p < 0.05$ was considered significant. SigmaStat for Windows, version 2.03, and SigmaPlot software were used for the statistical analysis. The data are expressed as the mean ± standard deviation (SD) of three independent experiments.

3. Results

The average primary sizes of Ag nanoparticles were verified by scanning electron microscopy (SEM), which showed spherical nanoparticles that increased in size in samples that were approximately 15, 30, and 55 nm (Figure 1). Once in suspension, these nanoparticles tended to agglomerate and rapidly settle out of solution. Therefore, initial dispersion tests were conducted in physiological phosphate-buffered saline (PBS, pH 7.4), deionized water, dimethylsulfoxide (DMSO), and ethanol (EtOH) to examine the behavior of the particles in various solutions. Based on the dispersion studies using physical mixing, that most stock suspensions of Ag-15nm, Ag-30nm, and Ag-55nm particles were prepared in deionized water. From these

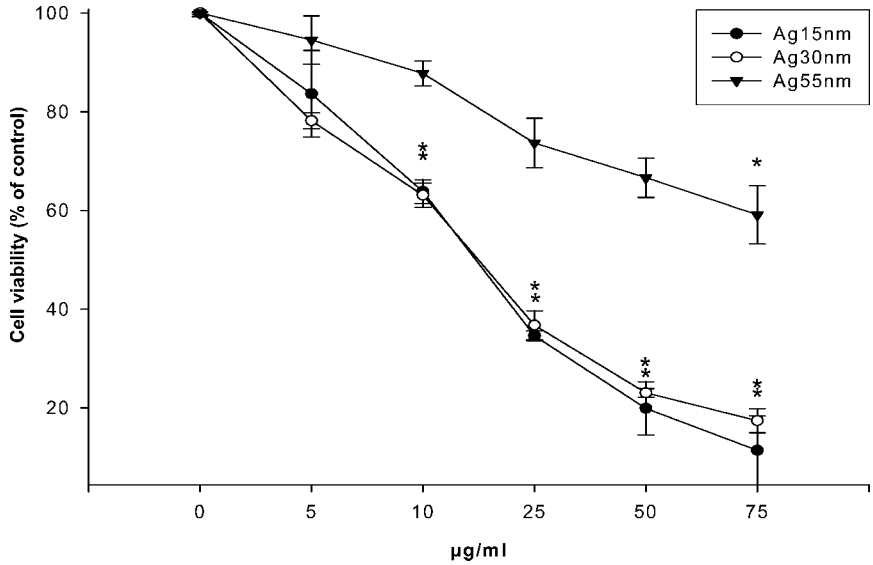

Figure 5. Effect of Ag nanoparticles on membrane integrity in macrophages. Cells were treated with various concentrations of silver nanoparticles for 24 h. Following the treatment period, membrane integrity was assessed by measuring LDH leakage with the CytoTOX-ONE Homogenous Membrane Integrity Assay kit. Fluorescence values of the control cells (nanoparticle-free exposure media) were set at 100%, and the fluorescence values of the treated cells were measured as percentages of the control. The data are expressed as the mean ± SD of three independent experiments conducted in triplicate. Asterisks (*) indicate a statistically significant difference compared to controls ($p < 0.05$). Both Ag-15nm and Ag-30nm significantly decreased cell viability at concentrations from 10 to 75 μg/mL, whereas Ag-55nm did not significantly reduce viability until 75 μg/mL.

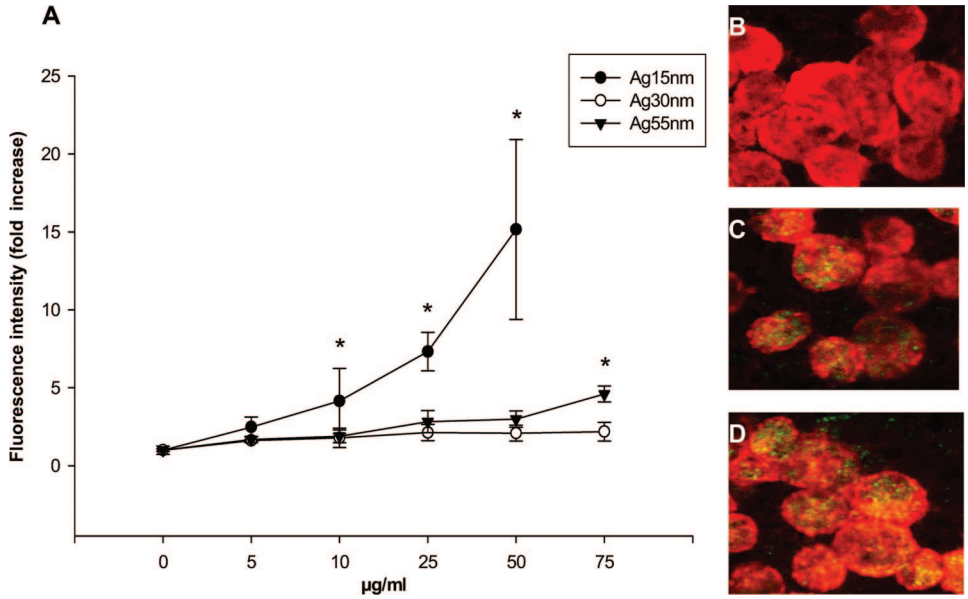

Figure 6. Effect of Ag nanoparticles on reactive oxygen species generation in macrophages. After 24 h of incubation with silver nanoparticles, the fluorescence intensity of dichlorofluorescein (DCF) was assessed by (A) microplate reader or (B−D) fluorescence microscopy. (A) Graph of mean data for ROS as fold increase in fluorescence ± SD relative to control cells (nanoparticle-free media) of three independent experiments. Asterisks (*) indicate a statistically significant difference compared to controls ($p < 0.05$). (B−D) Fluorescence microscopy images (200×) of cells following 24 h of treatment with Ag-15nm nanoparticles. (B) Control cells, (C) cells treated with 10 μg/mL Ag-15nm, and (D) cells treated with 25 μg/mL Ag-15nm. Notice the increase in ROS production in D (green fluorescence) with increased Ag-15nm concentration.

stock suspensions, final concentrations were prepared in Ham's Nutrient Mixture F-12K with 10% FBS and 1% P/S. Because turbidity increased with increasing concentration of nanomaterials, the highest dose was limited to 100 μg/mL.

Images captured by inverted light microscopy (100× magnification, oil) suggest nanoparticle attachment, internalization, and cellular damage after exposure to Ag nanoparticles compared to control cells (Figure 2). Control cells (Figure 2A−D) are shown as healthy and relatively symmetrical with sizes of approximately 10 μm. Following treatment with 25 and 75 μg/mL Ag-15nm, the cells lacked a defined plasma membrane and appeared shrunken, and cellular debris was floating in the medium (Figure 2E−L). Cells incubated with 25 and 75 μg/mL Ag-30nm appeared noticeably larger in size, with agglomerated nanoparticles both inside and outside the cells (Figure 2M−T). Cells incubated with 25 and 75 μg/mL Ag-55nm appeared clustered together, with large agglomerated nanoparticles on their surfaces and connecting between cells with little morphological changes compared to control cells. Further, it was noted that the silver nanoparticles were surrounded by the macrophages (not shown) when viewed at 20× magnification similar to Figure 2V,Z, suggesting that the cells were activated

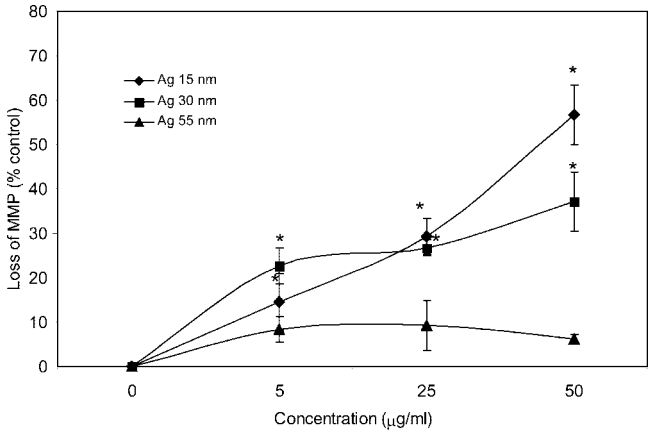

Figure 7. Assessment of mitochondrial membrane potential in macrophages. After 24 h of exposure to different concentrations of silver nanoparticles, cells were incubated with Mit-E-Ψ reagent and then examined for fluorescence intensity relative to control cells (100%) with microplate reading as described in Materials and Methods. Fluorescence intensity data expressed as percent of control as the mean ± SD of three independent experiments. Asterisks (*) indicate a statistically significant difference compared to time-matched controls ($p < 0.05$).

and working as per their phenotype to synergistically engulf agglomerates. However, it does not appear that many of the cells incubated with Ag-55nm successfully internalized the large agglomerates after 24 h because of a lack of dark areas inside the cells. Therefore, cells incubated with Ag-15nm appeared to undergo the greatest changes in cellular morphology indicative of toxicity compared to the control and Ag-30nm- and Ag-55nm-exposed cells. Of particular interest is the agglomeration of Ag-30nm and Ag-55nm nanoparticles, whereas Ag-15nm nanoparticles appeared less agglomerated in solution, which is supported by dispersion studies. Agglomerates greater than 10 μm are noticeable in images M, R, V, Z, and AA of Figure 2 even after techniques such as vortexing to disperse the initial suspension. Additionally, the degree of nanoparticle association with the membrane or amount of internalization was difficult to determine with light microscopy alone.

Macrophages are known to internalize 85−90% of cell-associated particles, so it is highly likely that the nanoparticles that were seen associated with the plasma membrane by phase-contrast light microscopy were internalized after 24 h. To further investigate the interaction of nanoparticles with alveolar macrophages, higher-resolution images were captured with the CytoViva Ultra Resolution Imaging (URI) system (Figure 3A,B) and with a transmission electron microscope (Figure 3C,D). Cells incubated with 25 μg/mL Ag-30nm nanoparticles for 24 h showed brightly illuminated areas in the cell with the CytoViva URI attachment, suggesting the presence of agglomerated nanoparticles inside the cell (Figure 3B). TEM images of the cells showed that 25 μg/mL Ag-55nm nanoparticles were also internalized by the cells after 24 h into vacuoles (Figure 3C,D). However, the mechanism of uptake was not investigated; therefore, it is unknown whether the nanoparticles were internalized as individual particles or taken up in an agglomerated form. The apparent limit on nanoparticle agglomerate size to less than 2 μm seen by TEM supports the hypothesis that large agglomerates (>10 μm) are not effectively internalized by the cells after 24 h.

The results of the MTT viability assay showed a significant decrease in mitochondrial function of alveolar macrophages exposed to Ag-15nm, Ag-30nm, or Ag-55nm nanoparticles for 24 h at concentrations ranging from 10 to 75 μg/mL (Figure 4A, Table 1). It was noted that 24 h of exposure to 50 μg/mL Ag-15nm resulted in an (88.66 ± 1.84)% decrease. Similarly, 24 h of exposure to 50 and 75 μg/mL Ag-30nm resulted in (69.72 ± 7.87)% and (91.15 ± 1.38)% decreases in mitochondrial function, respectively. Compared to the smaller nanoparticles (15 and 30 nm), Ag-55nm did not exhibit significant toxicity until 50−75 μg/mL, with only a (33.89 ± 7.89)% decrease at the highest dose (75 μg/mL). A relatively nontoxic nanoparticle control, TiO_2, was used to demonstrate that the toxic effects of Ag are unique to the material composition and not inherent to the nanosize (Figure 4B). After 24 h of exposure to 10−50 μg/mL TiO_2, there were no significant changes in viability compared to the untreated control cells for any of the TiO_2 nanoparticles, which were similar in size to the Ag nanoparticles (TiO_2-16nm, TiO_2-40nm, and TiO_2-50nm).

TABLE 1: Calculated EC_{50}[a] and CT[b] Values for Silver Nanoparticles

	MTT		LDH	
chemical	EC_{50} (μg/mL)	CT (μg/mL·h)	EC_{50} (μg/mL)	CT (μg/mL·h)
Ag-15nm	27.87 ± 12.23	668.88	14.75 ± 1.63	354.00
Ag-30nm	33.38 ± 11.48	801.12	13.89 ± 0.82	333.36
Ag-55nm	>75	—[c]	>75	—[c]
$AgNO_3$	27.38 ± 11.39	657.12	—[c]	—[c]
CdO	0.42 ± 0.13	10.08	4.27 ± 6.26	102.48

[a] EC_{50} values represent the effective concentration of silver nanoparticles required to decrease MTT reduction by 50% and increase LDH leakage by 50%. [b] CT values (EC_{50} X exposure time) represent the area under the exposure curve. [c] Could not be estimated.

The effective concentrations for toxicity at 50% cell loss (EC_{50} values) for MTT at 24 h were calculated as 27.87 ± 12.23 and 33.38 ± 11.48 μg/mL for the smaller nanoparticles, Ag-15nm and Ag-30nm, respectively (Table 1). The EC_{50} values for the larger nanoparticles were beyond the dose range (>100 μg/mL). CdO (1-μm particles) was used as a known positive control because of its ability to significantly decrease mitochondrial function after 24 h at very low doses (0.5 μg/mL). To compare the effects of metallic silver nanoparticles to a bulk soluble silver compound, $AgNO_3$ was assayed, and the data revealed similar toxic effects on mitochondrial function compared to Ag-15nm. At 50 μg/mL $AgNO_3$, (98.7 ± 0.5)% of exposed alveolar macrophages were nonviable.

After 24 h of exposure to Ag nanoparticles, decreases in cell viability were evaluated based on the release of LDH. As indicated in Figure 5, exposure to Ag nanoparticles resulted in a dose-dependent decrease in cell viability compared to control cells (0 μg/mL). Similarly to the MTT results, Ag-15nm and Ag-30nm exhibited significant ($p < 0.05$) cytotoxicity at 10−75 μg/mL, whereas Ag-55nm required a concentration of 75 μg/mL to significantly decrease cell viability. Data from 24-h exposures to silver nanoparticles showed that toxicity might be size-dependent. As measured by MTT and LDH assays, both Ag-15nm and Ag-30nm appeared toxic at low doses (~10 μg/mL). In comparison to the smaller sizes, Ag-55nm was the least toxic, decreasing cell viability by only ~41% at the highest dose (75 μg/mL).

To investigate the potential role of oxidative stress after 24 h of exposure to Ag-15nm, Ag-30nm, and Ag-55nm at 0, 5, 10, 25, 50, and 75 μg/mL exposures, the generation of reactive oxygen species (ROS) was measured, as shown in Figure 6. Exposure to Ag-15nm at concentrations of 25 and 50 μg/mL

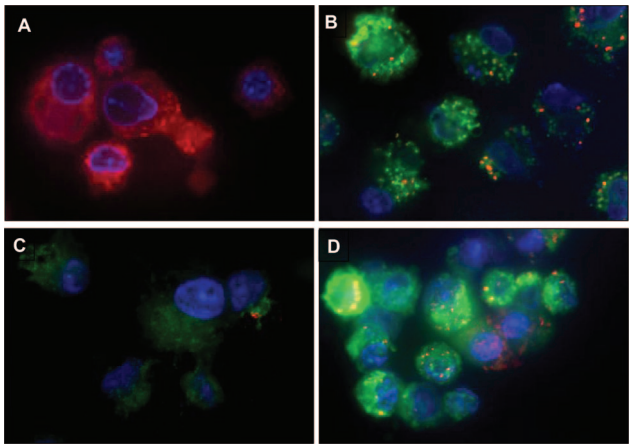

Figure 8. Confocal microscopy assessment of macrophages exposed to silver: normal vs apoptotic cells. After 24 h of exposure to different concentrations of silver nanoparticles, cells were incubated with Mit-E-Ψ reagent, and Hoescht 33342 stain was then imaged using the BD pathway 435 confocal microscope as described in Materials and Methods. (A) Control macrophages. Macrophages treated with 5 μg/mL (B) Ag-15nm, (C) Ag-30nm, and (D) Ag-55nm.

resulted in (7.32 ± 1.24)- and (15.16 ± 5.77)-fold increases, respectively, in ROS generation over control levels (Figure 6A). The qualitative generation of ROS was also observed using fluorescence microscopy, which detected the brightest fluorescence intensity in cells exposed to Ag-15nm at concentrations of 10 and 25 μg/mL (Figure 6C,D). Therefore, both qualitative and quantitative data confirm that exposure to Ag-15nm NPs induces the generation of ROS.

Mitochondrial membrane potential (MMP) was quantitatively evaluated to assess the further corollary of Ag-15nm nanoparticle exposure. Cells were exposed to 0, 5, 25, and 50 μg/mL Ag-15nm, Ag-30nm, and Ag-55nm for 24 h and immediately assayed for fluorescent dye (JC-1) uptake (Figure 7). The results indicated a significant losses of MMP (30% and 60%) at 25 and 50 μg/mL Ag-15nm (Figure 7), as well as losses upon exposure to Ag-30nm, whereas the greatest retention of MMP was observed with Ag-55nm. The mitochondrial membrane potential was altered in a size-dependent manner, and this loss of MMP function suggests that the mechanism of cell death observed in the earlier cell proliferation studies may be a result of mitochondrial driven apoptosis. Further studies would be required to determine the toxicity to be apoptosis or necrosis as NPs dose or exposure increases.

Figure 8 shows a qualitative assessment of macrophages exposed to Ag nanoparticles to distinguish normal cells from apoptotic cells. Cells incubated with Ag-15nm produced the greatest increase in apoptosis in a concentration-dependent manner, whereas Ag-55nm-treated cells showed the least amount of apoptosis when compared to the control cells (Figure 8). The Ag-30nm particles produced a response similar to that of the Ag-15nm nanoparticles at lower concentrations, but at the 50 μg/mL concentration, they induced less apoptosis than the Ag-15nm nanoparticles. This would indicate a size-dependent effect, with smaller silver nanoparticles inducing apoptosis more than larger nanoparticles. Figure 8A depicts the healthy control cells with no green fluorescence. Figure 8 B−D illustrates cells undergoing apoptosis after exposure to Ag nanoparticles at concentrations of 5 μg/mL. This low concentration was chosen for imaging because, at increasing concentrations, for the Ag-15nm nanoparticles, the cells detached and were washed away, thereby reducing the number of available cells to image.

TABLE 2: GSH Content in Macrophages after Silver Nanoparticle Exposure[a]

concentration (μg/mL)	GSH content (nmol/10^6 cells)			
	Ag-15nm	Ag-30nm	Ag-55nm	$AgNO_3$
0	6.96 ± 0.14	7.15 ± 0.15	6.41 ± 0.97	5.22 ± 0.39
10	4.72 ± 0.34	5.46 ± 1.10	4.84 ± 0.72	5.09 ± 0.33
50	0[b]	0[b]	4.84 ± 0.73	0[b]

[a] Rat alveolar macrophages were exposed to concentrations of silver nanoparticles for 24 h and analyzed for reduced glutathione (GSH) content in 96-well plates using a SpectraMAX Plus 190 microplate reader (Molecular Devices, Sunnyvale, CA) according to the procedures describe in the Glutathione Assay Kit #703002 (Cayman Chemical Company, Ann Arbor, MI). Values represent concentration (nmol) of GSH expressed per million cells. [b] Not detectable, below threshold limits.

GSH, a ubiquitous sulfhydryl-containing tripeptide, is the key antioxidant defense chemical that is responsible for maintaining cellular oxidation−reduction homeostasis.[21] Decreases in the levels of GSH can indicate functional damage to a cell. In this study, levels of GSH (nmol/10^6 cells) in alveolar macrophages exposed for 24 h to 50 μg/mL Ag-15nm, Ag-30nm, and $AgNO_3$ were completely depleted (Table 2). At a lower dose (10 μg/mL), Ag-15nm depleted GSH levels by 32.2%, whereas Ag-55nm did not appear to significantly deplete GSH levels at either dose.

Alveolar macrophages are stimulated to secrete inflammatory mediators, such as cytokines and chemokines, when exposed to foreign substances to enhance an immune response.[22] Therefore, we examined characteristic markers of macrophage activation, such as TNF-α, MIP-2, IL-1β, and IL-6, to determine whether rat alveolar macrophages respond to Ag-15nm, Ag-30nm, and Ag-55nm nanoparticles in a classical stimulatory fashion. The macrophages were exposed to 0, 5, 10, and 25 μg/mL Ag nanoparticles for 24 h. ELISA analysis of supernatants removed from exposed cells demonstrated that significant levels of TNF-α, MIP-2, and IL-1β were detected at 5, 10, and 25 μg/mL for all sizes of Ag nanoparticles when compared to control samples (Figure 9 A−C). However, cumulative cytokine production within this 24-h exposure showed no significant difference in cytokine secretion levels when comparing nanoparticle size with dosage level (Figure 9A−C). Unexpectedly, there was no detection of IL-6 in the supernatants of exposed cells at 6, 24, or even 48 h. In contrast, when the macrophages were exposed to 100 ng/mL LPS, the secretion levels of IL-6 increased dramatically (data not shown).

4. Discussion

In medical applications, silver is used for the treatment of burn and chronic wounds,[23] with new products containing nanosized silver being developed and introduced commercially. Silver nanoparticles have received considerable attention because of their attractive physicochemical properties when compared to different novel metal nanomaterials. The strong toxicity that silver exhibits in various chemical forms to a wide range of microorganisms is very well-known,[23,24] and silver nanoparticles have recently been shown to be a promising antimicrobial material.[25] However, in terms of the assessment of toxicological properties of nanoparticles, it is not known how they behave when they are dispersed in cell culture media over time and at different temperatures. The other issue that is still not known is whether the cells take up nanoparticles and, if so, what mechanisms are involved.

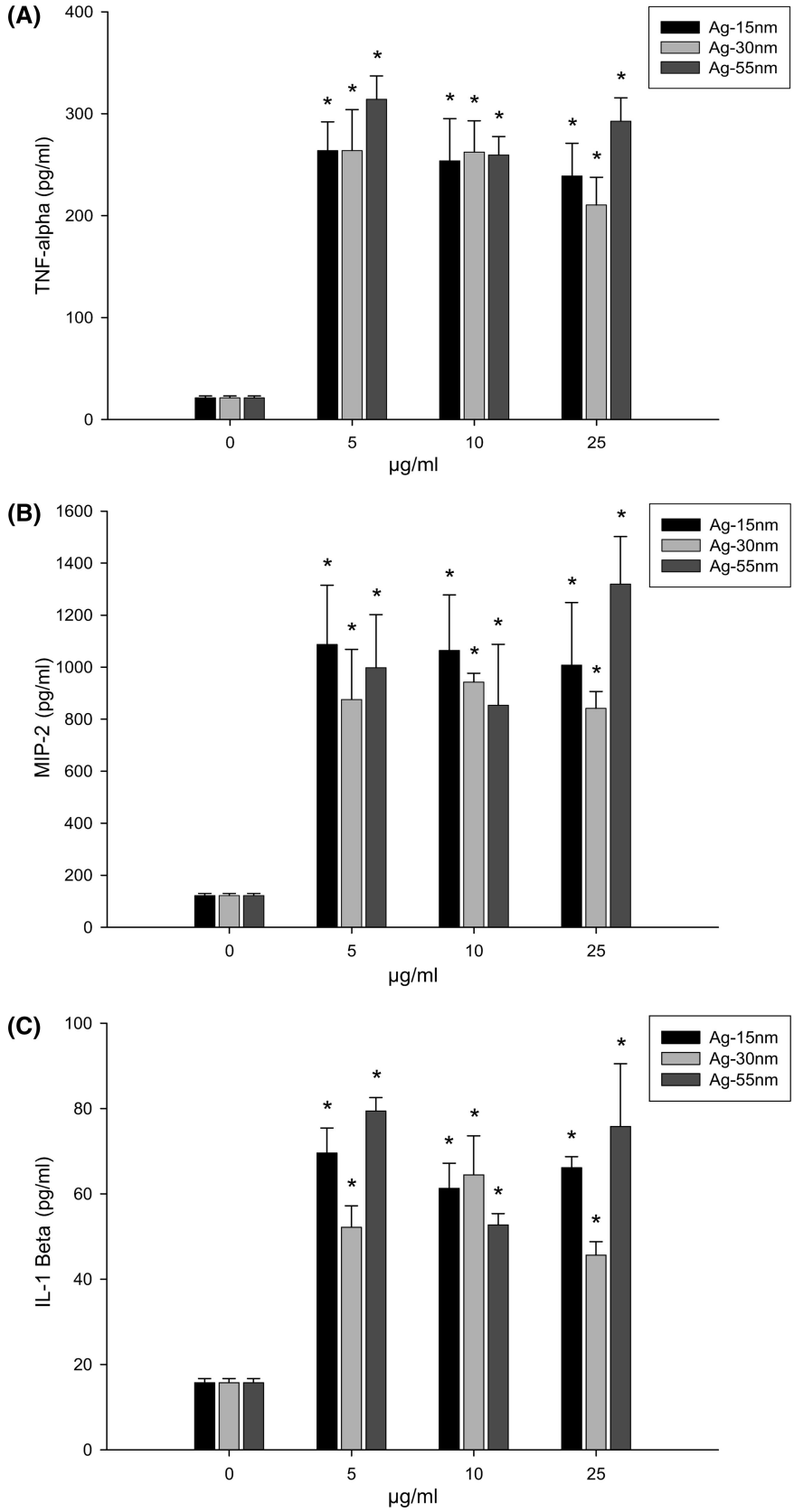

Figure 9. Proinflammatory response. Rat alveolar macrophages were exposed to 0, 5, 10, and 25 μg/mL Ag-15nm, Ag-30nm, or Ag-55nm nanoparticles for 24 h and analyzed for (A) TNF-α, (B) MIP-2, and (C) IL-1β levels within the control and exposed supernatants. Cytokines were determined by ELISA analysis. Asterisks (*) indicate a statistically significant difference compared to control samples ($p < 0.05$).

Before implementing the various applications of silver nanoparticles, it is necessary to investigate the potential toxicological impacts of silver nanomaterials. Currently, it is unclear how nanosilver interacts with and instigates toxicity in mammalian cells; however, there are some reports on nanosized silver activity toward bacteria and viruses. As reported by Elechiguerra et al.,[26] silver nanoparticles undergo a size-dependent interaction with HIV-1, where only silver

nanoparticles that are 1−10 nm can attach to the virus. In addition, Ag nanoparticles were found to be completely cytotoxic to *E. coli* for surface concentrations as low as 8 μg of Ag/cm^2.[27] In humans, ingested silver has been found to produce a medically benign bluish-gray discoloration of the skin called argyria.[25]

Limited studies are available that investigate the toxic effects of nanomaterials, and no clear guidelines are available to quantify these effects. Recently, Poland et al.[28] reported that carbon nanotubes introduced into the abdominal cavity of mice showed asbestos-like toxicity. Another report by Warheit et al.[29] investigated acute lung toxicity and observed that intratracheally instilled single-walled carbon nanotubes produced granulomas in rats at very high doses. We recently reported the cytotoxicities of different metal- or carbon-based nanoparticles in an in vitro model.[30−34] Although in vitro data are not a substitute for whole-animal studies, use of simple in vitro models with end points that reveal a general mechanism of toxicity can be a basis for further assessing the potential risk of chemical/material exposure. The present study aimed to investigate the general toxicity and interaction of silver nanoparticles with rat alveolar macrophages, as the size of the nanoparticles makes them unique and alters their behavior when compared to their bulk chemical counterpart or other nanoparticles of different compositions (e.g., TiO_2).

The Ag nanoparticles used in this study had surface hydrocarbons that did not form a continuous coating, but could be considered an artifact of the manufacturing process, which used hydrocarbons to prevent sintering of the Ag nanoparticles during plasma synthesis. Although Figure 1 describes the primary size of the Ag nanoparticles as measured by SEM, detailed studies of the size properties of Ag nanoparticles in cell culture media over time and at temperatures similar to those in the human body have not been performed to determine the actual size of agglomerates or individual nanoparticles that come into contact with the cells or are internalized.[31] Furthermore, surface area, dimensions, and surface energy might be important properties that contribute in some way to toxicity. Therefore, it would not be unreasonable as suggested by other investigators[35] to hypothesize that the toxicity of Ag nanoparticles could be based on the available exposed surface for reaction with the cell, which increases with decreasing nanoparticle size or increasing concentration of individual Ag nanoparticles per volume.

Our microscopy results showed that Ag nanoparticles associate with cell membranes and that the cells internalize some of the particles, which could have an effect on cellular function. Further examination of the internalized Ag nanoparticles revealed large aggregates that could be distinguished from other cellular components by their bright illumination resulting from intense light scattering or increased contrast with electron microscopy. The mechanism of Ag nanoparticle cellular entry can vary based on the cell type, and in these studies, it could involve a combination of large-scale phagocytosis of agglomerates or possibly a passive, nonspecific mechanism if individual nanoparticles can diffuse through the cell membrane. In either case, the solubility of the Ag nanoparticles in the cell membrane does not appear to be a factor for the uptake, and indeed, after 24 h, the Ag nanoparticles were found intact inside intracellular vesicles. However, modifying the surface properties of the Ag NPs (e.g., with hydrophobic/hydrophilic coatings) might prevent or limit their dispersion in solutions such as cell culture media, leading to reduced contact with the cell membrane and, therefore, preventing or limiting their uptake into the cell. Varying the coating and deactivation of metal nanoparticles for toxicity testing is not addressed in this study. As requirements for specific modified nanoproducts arise and consumer or worker exposure is inevitable, more research will be focused on this area.

In a previous study, we characterized surface properties of coated versus uncoated silver nanoparticles.[36] Silver nanoparticles remained intact,and there was no evidence of dissolution once inside the cells after 24 h of exposure because the nanoparticles remained approximately the same size both before and after incubation and uptake by the cells as measured with transmission electron microscopy (TEM). This is true even for Ag nanoparticles captured by the cells in what appears to be lysosomes or other cellular compartments destined for digestion. For example, size distributions performed by TEM showed spherical, nanometer-sized individual nanoparticles imaged from a dried solution or from thin cell sections that were previously incubated with the Ag NP solutions for 24 h. An example of the retention of Ag nanoparticles size once within the cell is shown in Figure 3D. Future studies could, however, attempt to examine the amount of soluble Ag and the surface state (e.g., charge, coating properties) of Ag nanoparticles inside the cells. However, this information is currently limited by the available characterization techniques. First, there is no reliable sample preparation procedure to effectively separate bound vs internalized vs solubilized nanosized Ag. Second, most extraction procedures to quantify trace amounts of metal [e.g., for inductively coupled plasma mass spectrometry (ICP-MS), AAS] rely on strong acids that can lead to artificial surface changes or dissolution of the nanoparticles and not represent the true state of NPs inside living cells or true external concentrations of solubilized metals. These are general limitations of research with nanosized particles, which are not fully soluble solutions of chemicals and therefore must be processed carefully by reviewing and revising the currently used toxicity protocols.

Using well-known toxicity tests in a slightly modified manner, Ag-15nm nanomaterials were found to increase LDH leakage and reduce MTT reduction in a dose-dependent manner over 24 h. However, it is unknown whether this compound has a significant dissolution rate within cultured cells or whether it gains access into the internal cellular matrix. Overall, the data based on MTT and LDH assays suggest that Ag nanoparticles exhibit a unique size-dependent toxicity. Further studies were conducted with silver particles to elucidate a general mechanism with reference to oxidative stress. The results reported here showed that there was a significant increase in ROS for 10, 25, and 50 μg/mL Ag-15nm. In correlation with increased ROS levels, GSH levels were completely depleted in cells exposed to Ag-15nm and 30 at a concentration of 50 μg/mL when compared to the larger-sized Ag-55nm particles. The detailed biochemical properties of silver inside the cells would provide more information to explain the differing results with different sizes. However, it is likely that GSH could be reduced by the direct interaction of the smaller, more reactive Ag nanoparticles and surface area available for reaction with GSH. Direct binding of the Ag nanoparticles to the GSH reductases or other GSH maintenance enzymes.

Increased generation of ROS and decreased levels of GSH by Ag-15nm support the hypothesis that the cells are undergoing oxidative stress, which could ultimately lead to the observed cytotoxicity. However, Ag-30nm particles induced cytotoxicity as indicated by MTT and LDH assays, but the level of ROS was not significantly increased in our measurements. When the size of the nanoparticles was increased, as for Ag-55nm, only marginal toxicity was indicated by both MTT and LDH assays. Although further study will be needed to investigate such differential cytotoxicity between Ag-15nm and Ag-30nm nanoparticles, the strong response elicited by Ag-15nm NPs is probably due to the total cell −SH

reactive nature, which might reduce the ability of the macrophage to protection from the production of ROS. Another possibility is that Ag-15nm might not have been quenched by glutathione, leading to a strong ROS generation, or exposure to Ag-15nm might induce apoptosis. The interesting observation in this study is that ROS uniquely associated with Ag-15nm nanoparticles compared to similar sizes of other nanoparticles such as aluminum[11,34] and silica (unpublished data). The production of ROS was absent after exposure to 2−10-nm diamond nanoparticles[33] compared to carbon nanotubes,[33] and we have also observed that silica nanoparticles display size-dependent toxicity but do not induce ROS (unpublished data). The increased secretion of inflammatory cytokines/chemokines appeared for all sizes of silver but was not size-dependent. Only 24 hr cumulative inflammatory protein amounts were reported here. Differences between Ag Np could occur temporarlly and change expression dynamics between cytokines would require further in depth studies. However, it appears that this ROS effect is unique to Ag nanoparticles. This could be explained by the reactive nature of Ag-15nm at the nanoscale, and it might hinder the macrophage's protective mechanisms from subsequent ROS generation. This preliminary data suggest that oxidative stress is likely to contribute to nanoparticle cytotoxicity for the 15-nm silver nanoparticles. Further study is required to characterize the nature of silver inside cells. Because silver is an attractive component in many applications, it is necessary to understand the biological nature of nanosilver metal to assess its benefits and risks. The present study attempts to elucidate a portion of the biological properties and provide material scientists with aspects that are important in physicochemical properties such as coating, size, and surface properties to reduce the toxicity of silver nanoparticles and create biocompatible products.

Acknowledgment. This work was supported by the Air Force Office of Scientific Research (AFOSR) Project JON 2312A211. A.M.S. was funded by the Biosciences and Protection Division, Air Force Research Laboratory, under the Oak Ridge Institute for Science and Education (ORISE) and the Dayton Area Graduate Studies Institute (DAGSI). L.B.-S., a postdoctoral fellow, was supported by National Research Council under the AFOSR program. We are also thankful to our Division Chief Col Riddle for his strong support and encouragement and contributions from the Biological Interactions of Nanomaterials (BIN) group members.

References and Notes

(1) Bruchez, M., Jr.; Moronne, M.; Gin, P.; Weiss, S.; Alivisatos, A. P. Semiconductor nanocrystals as fluorescent biological labels. *Science* **1998**, *281*, 2013–2016.

(2) Cui, Y.; Wei, Q.; Park, H.; Lieber, C. M. Nanowire nanosensors for highly sensitive and selective detection of biological and chemical species. *Science* **2001**, *293*, 1289–1292.

(3) Taton, T. A.; Mirkin, C. A.; Letsinger, R. L. Scanometric DNA array detection with nanoparticle probes. *Science* **2000**, *289*, 1757–1760.

(4) Brown, D. M.; Wilson, M. R.; MacNee, W.; Stone, V.; Donaldson, K. Size-dependent proinflammatory effects of ultrafine polystyrene particles: A role for surface area and oxidative stress in the enhanced activity of ultrafines. *Toxicol. Appl. Pharmacol.* **2001**, *175*, 191–199.

(5) Muller, M.; Mackeben, S.; Muller-Goymann, C. C. Physicochemical characterisation of liposomes with encapsulated local anaesthetics. *Int. J. Pharm.* **2004**, *274*, 139–148.

(6) Foley, S.; Crowley, C.; Smaihi, M.; Bonfils, C.; Erlanger, B. F.; Seta, P.; Larroque, C. Cellular localisation of a water-soluble fullerene derivative. *Biochem. Biophys. Res. Commun.* **2002**, *294*, 116–119.

(7) Alt, V.; Bechert, T.; Steinrucke, P.; Wagener, M.; Seidel, P.; Dingeldein, E.; Domann, E.; Schnettler, R. An *in vitro* assessment of the antibacterial properties and cytotoxicity of nanoparticulate silver bone cement. *Biomaterials* **2004**, *25*, 4383–4391.

(8) Panacek, A.; Kvitek, L.; Prucek, R.; Kolar, M.; Vecerova, R.; Pizurova, N.; Sharma, V. K.; Nevecna, T.; Zboril, R. Silver colloid nanoparticles: synthesis, characterization, and their antibacterial activity. *J. Phys. Chem. B* **2006**, *110*, 16248–16253.

(9) Lok, C. N.; Ho, C. M.; Chen, R.; He, Q. Y.; Yu, W. Y.; Sun, H.; Tam, P. K.; Chiu, J. F.; Che, C. M. Silver nanoparticles: Partial oxidation and antibacterial activities. *J. Biol. Inorg. Chem.* **2007**, *12*, 527–534.

(10) Hussain, S.; Meneghini, E.; Moosmayer, M.; Lacotte, D.; Anner, B. M. Potent and reversible interaction of silver with pure Na,K-ATPase and Na,K-ATPase-liposomes. *Biochim. Biophys. Acta* **1994**, *1190*, 402–408.

(11) Hussain, S. M.; Hess, K. L.; Gearhart, J. M.; Geiss, K. T.; Schlager, J. J. *In vitro* toxicity of nanoparticles in BRL 3A rat liver cells. *Toxicol. In Vitro* **2005**, *19*, 975–983.

(12) Braydich-Stolle, L.; Hussain, S.; Schlager, J. J.; Hofmann, M. C. *In vitro* cytotoxicity of nanoparticles in mammalian germline stem cells. *Toxicol. Sci.* **2005**, *88*, 412–419.

(13) Colvin, V. L. The potential environmental impact of engineered nanomaterials. *Nat. Biotechnol.* **2003**, *21*, 1166–1170.

(14) Oberdorster, E. Manufactured nanomaterials (fullerenes, C_{60}) induce oxidative stress in the brain of juvenile largemouth bass. *Environ. Health Perspect.* **2004**, *112*, 1058–1062.

(15) Jani, P.; Halbert, G. W.; Langridge, J.; Florence, A. T. Nanoparticle uptake by the rat gastrointestinal mucosa: Quantitation and particle size dependency. *J. Pharm. Pharmacol.* **1990**, *42*, 821–826.

(16) Lipscomb, M. F. Lung defenses against opportunistic infections. *Chest* **1989**, *96*, 1393–1399.

(17) Lee, K. P.; Trochimowicz, H. J.; Reinhardt, C. F. Pulmonary response of rats exposed to titanium dioxide (TiO_2) by inhalation for two years. *Toxicol. Appl. Pharmacol.* **1985**, *79*, 179–192.

(18) Carmichael, J.; DeGraff, W. G.; Gazdar, A. F.; Minna, J. D.; Mitchell, J. B. Evaluation of a tetrazolium-based semiautomated colorimetric assay: assessment of chemosensitivity testing. *Cancer Res.* **1987**, *47*, 936–942.

(19) Wang, H.; Joseph, J. A. Quantifying cellular oxidative stress by dichlorofluorescein assay using microplate reader. *Free Radicals Biol. Med.* **1999**, *27*, 612–616.

(20) Wu, E. Y.; Smith, M. T.; Bellomo, G.; Di, M. D. Relationships between the mitochondrial transmembrane potential, ATP concentration, and cytotoxicity in isolated rat hepatocytes. *Arch. Biochem. Biophys.* **1990**, *282*, 358–362.

(21) Sies, H. Glutathione and its role in cellular functions. *Free Radicals Biol. Med.* **1999**, *27*, 916–921.

(22) Lomas-Neira, J. L.; Chung, C. S.; Wesche, D. E.; Perl, M.; Ayala, A. *In vivo* gene silencing (with siRNA) of pulmonary expression of MIP-2 versus KC results in divergent effects on hemorrhage-induced, neutrophil-mediated septic acute lung injury. *J. Leukoc. Biol.* **2005**, *77*, 846–853.

(23) Liau, S. Y.; Read, D. C.; Pugh, W. J.; Furr, J. R.; Russell, A. D. Interaction of silver nitrate with readily identifiable groups: Relationship to the antibacterial action of silver ions. *Lett. Appl. Microbiol.* **1997**, *25*, 279–283.

(24) Nomiya, K.; Yoshizawa, A.; Tsukagoshi, K.; Kasuga, N. C.; Hirakawa, S.; Watanabe, J. Synthesis and structural characterization of silver(I), aluminium(III) and cobalt(II) complexes with 4-isopropyltropolone (hinokitiol) showing noteworthy biological activities. Action of silver(I)−oxygen bonding complexes on the antimicrobial activities. *J. Inorg. Biochem.* **2004**, *98*, 46–60.

(25) Sondi, I.; Salopek-Sondi, B. Silver nanoparticles as antimicrobial agent: A case study on *E. coli* as a model for Gram-negative bacteria. *J. Colloid Interface Sci.* **2004**, *275*, 177–182.

(26) Elechiguerra, J. L.; Burt, J. L.; Morones, J. R.; Camacho-Bragado, A.; Gao, X.; Lara, H. H.; Yacaman, M. J. Interaction of silver nanoparticles with HIV-1. *J. Nanobiotechnology* **2005**, *3*, 6.

(27) Baker, C.; Pradhan, A.; Pakstis, L.; Pochan, D. J.; Shah, S. I. Synthesis and antibacterial properties of silver nanoparticles. *J. Nanosci. Nanotechnol.* **2005**, *5*, 244–249.

(28) Poland, C. A.; Duffin, R.; Kinloch, I.; Maynard, A.; Wallace, W. A. H.; Seaton, A.; Stone, V.; Brown, S.; Macnee, W.; Donaldson, K. Carbon nanotubes introduced into the abdominal cavity of mice show asbestos-like pathogenicity in a pilot study. *Nat. Nanotechnol.* **2008**, *3*, 423–428.

(29) Warheit, D. B.; Laurence, B. R.; Reed, K. L.; Roach, D. H.; Reynolds, G. A.; Webb, T. R. Comparative pulmonary toxicity assessment of single-wall carbon nanotubes in rats. *Toxicol. Sci.* **2004**, *77*, 117–125.

(30) Murdock, R. C.; Braydich-Stolle, L.; Schrand, A. M.; Schlager, J. J.; Hussain, S. M. Characterization of Nanomaterial Dispersion in Solution Prior to In Vitro Exposure Using Dynamic Light Scattering Technique. *Toxicol. Sci.* **2008**, *101*, 239–253.

(31) Hussain, S.; Javorina, A.; Schrand, A.; Duhart, H.; Ali, S.; Schlager, J. The Interaction of Manganese Nanoparticles with PC-12 Cells Induces Dopamine Depletion. *Toxicol. Sci.* **2006**, *92* (2), 456–463.

(32) Grabinski, C.; Hussain, S.; Lafdi, K.; Braydich-Stolle, L.; Schlager, J. J. Effect of Particle Dimension on Biocompatibility of Carbon Nanomaterials. *Carbon* **2007**, *45*, 2828–2835.

(33) Schrand, A. M.; Huang, H.; Carlson, C.; Schlager, J. J.; Ōsawa, E.; Hussain, S. M.; Dai, L. Are Diamond Nanoparticles Cytotoxic? *J. Phys. Chem. B* **2007**, *111*, 2–7.

(34) Wagner, A. J.; Bleckmann, C. A.; Murdock, R. C.; Schrand, A. M.; Schlager, J. J.; Hussain, S. M. Cellular interaction of different forms of aluminum nanoparticles in rat alveolar macrophages. *J. Phys. Chem. B* **2007**, *111*, 7353–7359.

(35) Oberdöster, G.; Oberdörster, E.; Oberdörster, J. *Concepts of Nanoparticles Dose Metric and Response Metric Environ Health Perspect* **2007**, *115*, 187–194.

(36) Schrand, A. M.; Braydich-Stolle, L. K.; Schlager, J. J.; Dai, L.; Hussain, S. M. Can silver nanoparticles be useful as potential biological labels? *Nanotechnology* **2008**, *19*, 235104.

JP712087M